THE JOURNAL OF BIOLOGICAL CHEMISTRY VOL. 290, NO. 18, pp. 11591–11600, May 1, 2015


# Zinc Inhibits Hedgehog Autoprocessing

## *LINKING ZINC DEFICIENCY WITH HEDGEHOG ACTIVATION**

Received for publication, November 2, 2014, and in revised form, March 12, 2015 Published, JBC Papers in Press, March 18, 2015, DOI 10.1074/jbc.M114.623264

**Jian Xie[‡§], Timothy Owen[¶], Ke Xia[‖], Ajay Vikram Singh[**], Emiley Tou[‡‡], Lingyun Li[‖], Brigitte Arduini[§], Hongmin Li[§§], Leo Q. Wan[§**1], Brian Callahan[¶], and Chunyu Wang[‡§‖‡‡2]**

*From the [‡]Biochemistry and Biophysics Graduate Program, [‖]Department of Chemistry and Chemical Biology, **Department of Biomedical Engineering, and [‡‡]Department of Biological Sciences, [§]Center for Biotechnology and Interdisciplinary Studies, Rensselaer Polytechnic Institute, Troy, New York 12180, [¶]Department of Chemistry, Binghamton University, Binghamton, New York 13902, and [§§]Wadsworth Center, New York State Department of Health, Albany, New York 12208*

**Background:** In many types of cancers zinc deficiency and overproduction of Hedgehog (Hh) ligand co-exist.
**Results:** Zinc binds to the active site of the Hedgehog-intein (Hint) domain and inhibits Hh ligand production both *in vitro* and in cell culture.
**Conclusion:** Zinc influences the Hh autoprocessing.
**Significance:** This study uncovers a novel mechanistic link between zinc and the Hh signaling pathway.

**Zinc is an essential trace element with wide-ranging biological functions, whereas the Hedgehog (Hh) signaling pathway plays crucial roles in both development and disease. Here we show that there is a mechanistic link between zinc and Hh signaling. The upstream activator of Hh signaling, the Hh ligand, originates from Hh autoprocessing, which converts the Hh precursor protein to the Hh ligand. In an *in vitro* Hh autoprocessing assay we show that zinc inhibits Hh autoprocessing with a $K_i$ of 2 $\mu$M. We then demonstrate that zinc inhibits Hh autoprocessing in a cellular environment with experiments in primary rat astrocyte culture. Solution NMR reveals that zinc binds the active site residues of the Hh autoprocessing domain to inhibit autoprocessing, and isothermal titration calorimetry provided the thermodynamics of the binding. In normal physiology, zinc likely acts as a negative regulator of Hh autoprocessing and inhibits the generation of Hh ligand and Hh signaling. In many diseases, zinc deficiency and elevated level of Hh ligand co-exist, including prostate cancer, lung cancer, ovarian cancer, and autism. Our data suggest a causal relationship between zinc deficiency and the overproduction of Hh ligand.**

Hedgehog (Hh)[3] signaling pathway regulates cell proliferation, tissue polarity, and cell differentiation during normal development (1). Abnormal signaling of this pathway has been reported in a variety of human diseases, including cancer and neurodevelopmental diseases. For example, chronic Hh pathway stimulation is observed in prostate cancer (2–4), lung cancer (5, 6), and ovarian cancer (7, 8) in a Hh ligand-dependent manner. Recently, serum levels of Hh ligand protein were found to be significantly higher in children with autism spectrum disorder (ASD) and the levels of Hh ligand were correlated with the severity of autism (9). However, the mechanisms of Hh ligand overproduction in these diseases are poorly understood.

Hh ligand is generated from a precursor protein composed of an N-terminal signaling domain (HhN) and a C-terminal autoprocessing (HhC) domain (Fig. 1*A*), through intein-like chemistry catalyzed by the Hint (Hedgehog/intein) domain within HhC. During Hh autoprocessing, HhC cleaves HhN from the precursor and covalently links a cholesterol molecule to the C terminus of HhN. HhN is also palmitoylated at the N terminus by the Hedgehog acyl transferase (10). The double lipidation of HhN is required for proper Hh ligand transportation and downstream signaling (11). Because zinc inhibits intein-mediated protein splicing (12) and HhC is homologous to inteins (13), we reasoned that zinc may also suppress Hh autoprocessing and the generation of Hh ligand.

Interestingly, zinc deficiency has been well documented in many diseases with elevated level of Hh ligand (14–21) both in patient serum and affected tissues. If zinc normally inhibits Hh autoprocessing, low zinc level can potentially enhance Hh autoprocessing and increase the level of Hh ligand in these diseases, contributing to their pathogenesis. However, the mechanistic link between zinc and Hh signaling has not been characterized previously. In this study we demonstrate that zinc binds directly to the active site of Hint domain and inhibits the autoprocessing of Hh precursor both *in vitro* and in cell culture, uncovering a novel connection between two essential pathways in many physiological and pathological processes.

## EXPERIMENTAL PROCEDURES

*DNA Constructs*—The expression plasmid, pET22b-SHhN-DHhC, encoding HhN of human Sonic Hh fused to HhC of *Drosophila melanogaster* was prepared by ligating the corresponding synthetic gene fusion (Genscript) into pET22b (Novagen) using unique NdeI and HindIII sites (Fig. 1*B*). For

* This work was supported, in whole or in part, by National Institutes of Health Grant R01GM081408 (NIGMS; to C. W.). This work was also supported in part through Department of Defense Grant W81XWH-14-1-0155 (to B. C.).
[1] A Pew Scholar in Biomedical Sciences, supported by the Pew Charitable Trusts.
[2] To whom correspondence should be addressed: Biochemistry and Biophysics Graduate Program, Dept. of Chemistry and Chemical Biology and Dept. of Biological Sciences, Rensselaer Polytechnic Institute, 110 8th street, Troy, NY. Tel.: 518-276-3497; E-mail: wangc5@rpi.edu.
[3] The abbreviations used are: Hh, Hedgehog; Hint, Hedgehog-intein; ASD, autism spectrum disorder; HA, hydroxylamine; HSQC, heteronuclear single quantum correlation; ITC, isothermal titration calorimetry; SMO, Smoothened; N-S acyl shift, nitrogen to sulfur acyl shift.

pET45b $His_6$-shortened Hh precursor, the coding sequence for *D. melanogaster* HhC fragment was PCR-amplified from genomic DNA, digested with KpnI and HindIII, and ligated into pET45b to generate an N-terminal His-tagged construct (see Fig. 3*A*). Primers sequences, with restriction sites underlined were as follows: forward, TTTCACGTGGGTACCGGTGAAAACCTGTATTTTCAGGGCTCGACGGTGCATGGCTGCTTC; reverse, TTTAAGCTTAATCGTGGCGCCAGCTCTGCGGCAGAACG.

*Protein Expression and Purification*—All non-labeled cells were grown at 37 °C in *Escherichia coli* strain BL21 (DE3) and induced with 1 mM isopropyl β-D-1-thiogalactopyranoside at

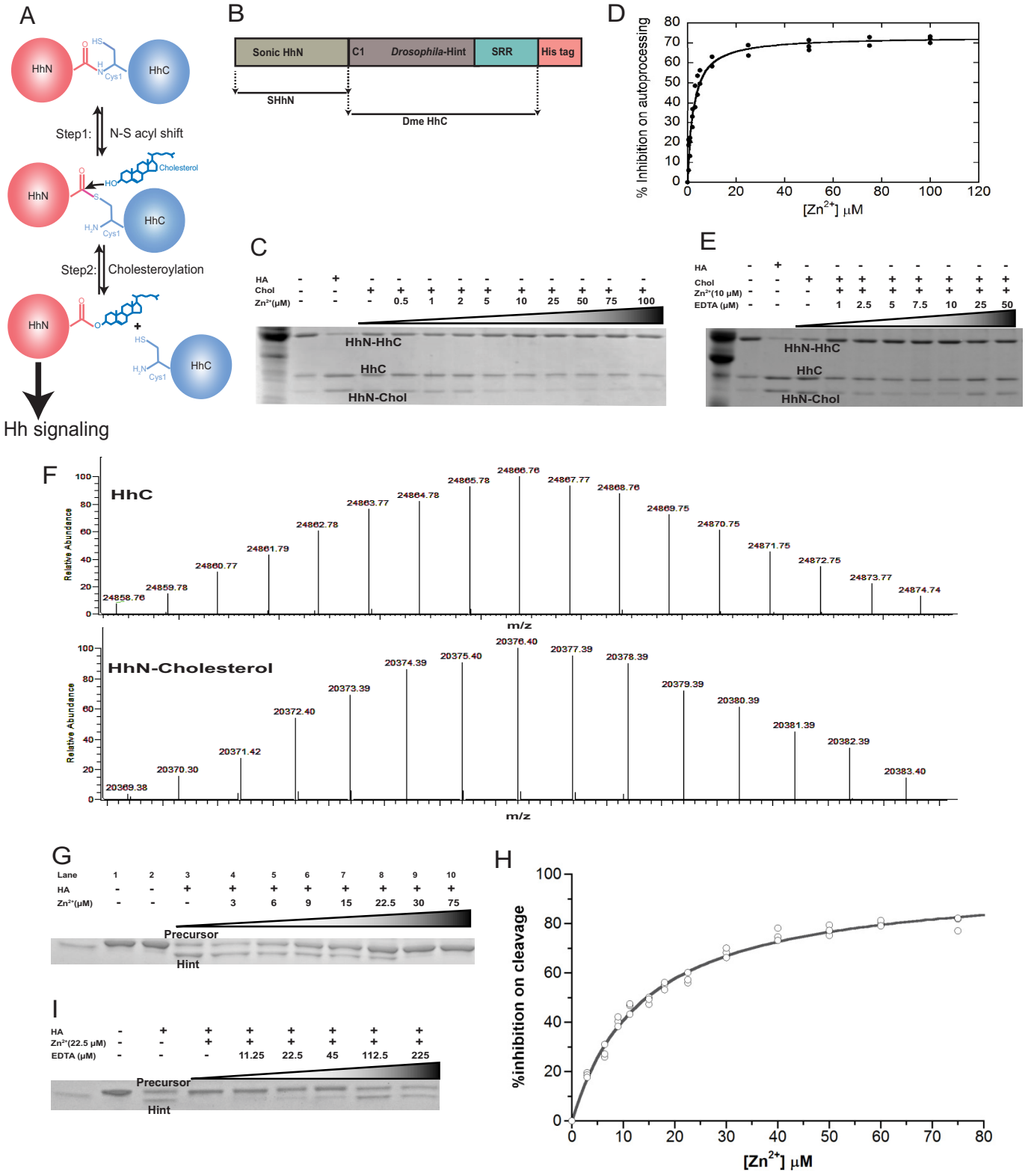

an $A_{600}$ of ~0.5 and then incubated at 20 °C overnight. Cells were lysed by B-per lysis buffer (Thermo Scientific, Waltham, MA) and purified by nickel-nitrilotriacetic acid chromatography. Hint domain was cleaved from the shortened precursor with 200 mM dithiothreitol (DTT) at 25 °C overnight. Affinity chromatography was utilized again to trap the $His_6$ tag, and uncleaved fusion protein and flow-through fractions were pooled. The pure protein was exchanged by dialysis into a buffer containing 50 mM Tris, pH 7.1, 100 mM NaCl, and concentrated by ultrafiltration with Amicon Ultra Centrifugal Filter Devices (Millipore Corp.; 10-kDa molecular weight cutoff). NMR sample preparation for Hint was described previously (22).

*In Vitro Autoprocessing Assays and Zinc Treatment*—Autoprocessing reactions contain ~0.16 mg/ml SHhN-DHhC precursor in incubation buffer (50 mM Tris, 100 mM NaCl, pH 7.1) with or without cholesterol (500 $\mu$M final concentration). The reactions were incubated at 25 °C and were stopped after 1 h by adding SDS-PAGE sample buffer (without $\beta$-mercaptoethanol). The samples were separated by SDS-PAGE. N-S acyl shift reactions contained ~0.25 mg/ml shortened Hh precursor, composed of a His tag, four HhN residues, HVHG, and *Drosophila*-Hint (see Fig. 3*A*) in incubation buffer (50 mM Tris, 100 mM NaCl, pH 7.1) with or without hydroxylamine (HA) (200 mM final concentration). The reactions were incubated at 25 °C and were stopped after 3 h by adding SDS-PAGE sample buffer (without $\beta$-mercaptoethanol). The samples were analyzed by SDS-PAGE.

For zinc inhibition assay on cholesteroylation, the Hh protein was incubated with cholesterol (500 $\mu$M final concentration) and various concentration of zinc (0.5–100 $\mu$M $ZnCl_2$) at 25 °C for 1 h. EDTA was used to as the chelator for zinc. Hh autoprocessing was monitored by SDS-PAGE. For the zinc inhibition assay on N-S acyl shift, the shortened Hh precursor, as depicted in Fig. 3*A*, was incubated with 200 mM HA and various concentrations of zinc (3–75 $\mu$M $ZnCl_2$) at 25 °C for 3 h. EDTA was used to as the chelator for zinc. Hh N-S acyl shift was monitored by SDS-PAGE.

Dose-response curves and $K_i$ values for both cholesteroylation and N-S acyl shift were determined by fitting the data with four parameter logarithmic nonlinear regression analysis with KaleidaGraph software. The dose-response equation we used was,

$$\text{Activity}_{\text{calc}} = (\text{max} \times [Zn^{2+}])/(K_i + [Zn^{2+}]) \quad \text{(Eq. 1)}$$

*Liquid Chromatography (LC)-Mass Spectrometry*—Protein samples were diluted to 25 $\mu$g/ml and analyzed using an Agilent 1200-Series LC system coupled to an LTQ-Orbitrap mass spectrometer (Thermo Scientific). For Fig. 1*F*, the LC system was equipped with a 2.1-mm inner diameter, 100-mm HPLC column packed with 5 $\mu$m BioBasic, C18, 300 Å resin (Thermo Scientific). Elution was achieved with a gradient of 5–90% B (98% acetonitrile in 1% formic acid) in 15 min. The flow rate was 0.2 ml/min.

*ITC Titrations*—Isothermal titration calorimetry measurements were obtained at 25 °C with an ITC200 MicroCal MCS titration microcalorimeter. Typically, 30 or 50 portions of 5 $\mu$l of $ZnCl_2$ solution were injected into the protein in the sample cell during each titration. The delay between injections (300 s) was sufficiently long for the thermal equilibrium before the next injection. The heat released by the interaction was measured by the instrument. Heat of dilution was obtained from a control titration of zinc into buffer alone under the same conditions. All experiments were repeated three times. Integrated heat data corrected for heats of dilution were fitted with a nonlinear least-squares minimization algorithm to a theoretical titration curve, with the Origin software package supplied by MicroCal. The ITC data are presented by showing the baseline-adjusted experimental titration (heat flow *versus* time) on the top and the peak-integrated concentration-normalized molar heat flow per aliquot *versus* the titrant-to-sample molar ratio on the bottom (Fig. 3). The solid line in the bottom plot represents the best fit of the data to the one-site equilibrium binding expression.

*NMR Spectroscopy*—All NMR experiments were carried out at 298 K on a Bruker 800 MHz spectrometer equipped with a cryogenic probe. Spectra were processed with nmrPipe software (23) and analyzed using Sparky (T. D. Goddard and D. G. Kneller, SPARKY 3, University of California, San Francisco, CA). The $^1H$ chemical shifts were referenced relative to DSS (2,2-dimethyl-2-silapentanesulfonic acid), and the $^{15}N$ and $^{13}C$ chemical shifts were referenced indirectly. The complete backbone and aliphatic side chain assignment of Hint has been published (22). The assignment of histidines were based on the (H$\beta$)C$\beta$(C$\gamma$C$\delta$)H$\delta$ spectrum, which connects C$\beta$ to H$\delta$ in the imidazole ring.

Chemical shift perturbation on backbone was monitored using $^1H$,$^{15}N$-HSQC spectra at increasing molar ratios of zinc to Hint. To monitor the zinc binding on cysteines (Cys-1 and

FIGURE 1. **Zinc inhibits Hh autoprocessing *in vitro*.** *A*, Hh autoprocessing mechanism. Hh is composed of two domains, the N terminus signaling domain (*HhN*) and C terminus autoprocessing domain (*HhC*). In the first step N-S acyl shift, the thiol group of Cys-1 initiates a nucleophilic attack on the carbonyl carbon of the preceding residue, Gly-(−1). This attack results in replacement of the peptide bond between Gly-1 and Cys-1 by a thioester linkage. In the second step cholesteroylation, the thioester is subject to a second nucleophilic attack from the hydroxyl group of a cholesterol molecule bound by the sterol recognition region (*SRR*) within HhC, resulting in a cholesterol-modified HhN and a free HhC. *B*, schematic diagram of the construct for cholesteroylation assay, composed of both HhN and HhC. It is a chimera fusion protein that contains SHhN at its N terminus and *Drosophila melanogaster* HhC at its C terminus. *C*, zinc inhibits Hh cholesteroylation *in vitro*. HA can induce the N-S acyl shift and initiate the cleavage of Hh. *Chol*, cholesterol; $Zn^{2+}$: $ZnCl_2$. *D*, quantitative analysis of zinc inhibition on Hh autoprocessing *in vitro*. The experiments were repeated 3 times, and the $K_i$ was 2.3 ± 0.2 $\mu$M. *E*, EDTA reversal of zinc inhibition in cholesteroylation assay. *F*, LC/electrospray ionization-MS analysis of the products of the autoprocessing assay, cleaved HhC and cholesteroylated HhN. The *upper portion* shows one of the reaction products, the *Drosophila melanogaster* HhC. The calculated average mass ($mass_{average}$ = 24867.29 Da) is between the two most abundant peaks in our experimental spectrum. The *bottom portion* shows the correct mass for cholesterol-modified SHhN ($mass_{average}$ = 20377.15 Da). These data proved the cholesteroylation of HhC in our assay. *G*, zinc inhibits HA-induced N-S acyl shift at 25 °C for 3 h. HA can cleave the thioester formed by N-S acyl shift in shortened Hh precursor, which lacks sterol recognition region. *Lane 1* is the precursor at 4 °C, and *lane 2* is the precursor at 25 °C, which shows the precursor is stable at both temperatures for at least 3 h. *H*, quantitative analysis of zinc inhibition on Hh N-S acyl shift. The experiments were repeated 3 times, and $K_i$ was calculated to be 14 ± 1 $\mu$M. *I*, EDTA reversal of zinc inhibition in N-S acyl shift.

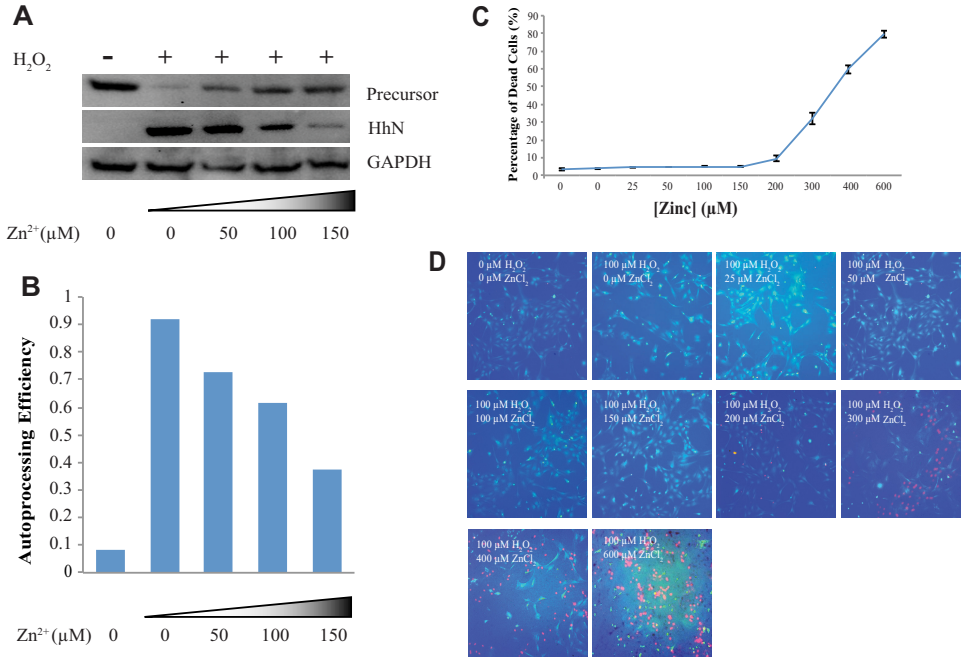


FIGURE 2. **Zinc inhibits Hh autoprocessing in primary astrocyte cell culture.** *A*, zinc inhibits Hh autoprocessing in astrocytes. Immunoblotting for GAPDH was used as a loading control. *B*, quantitative analysis was performed with ImageJ. The amounts of proteins were normalized to those of GAPDH. *C*, dose-response curve for percentage of dead rat primary astrocyte cells by varying concentrations of environmental zinc. Cultures were exposed to 0–600 μM zinc and 100 μM $H_2O_2$ for 40 h. The cell viability was assessed using the Live/Dead cell imaging kit, and the percentage of dead cells was determined by the Spot Detector BioApplication. Results are expressed as the mean derivations ± S.D. for two cultures. *D*, a representative figure for each condition. In each figure green fluorescence represents live cells and red fluorescence represents dead cells.

Cys-143), aspartic acid (Asp-46), and histidine (His-72) side chains, $^{13}C$,$^{1}H$-HSQC, two dimensional HB(CB)CO, and aromatic $^{13}C$,$^{1}H$-HSQC spectra were acquired separately.

*Culture of Primary Astrocytes*—Primary astrocyte cultures were prepared from the cerebral cortex of newborn Sprague-Dawley rats as previously described (24, 25). All animal procedures in this study strictly adhered to the National Institutes of Health Guidelines for the Care and Use of Laboratory Animals and were approved by the Institutional Animal Care and Use Committee of Rensselaer Polytechnic Institute. Postnatal 1-day-old rat pups were euthanized by rapid decapitation. The cerebral cortices were separated from the meninges, hippocampi, and basal ganglia. The cortical tissue from four animals was dissociated in Opti-MEM (Invitrogen) and transferred into a solution containing a 1:1 mix of recombinant protease TrypLE and Opti-MEM (Invitrogen). Cells were separated from the tissue using three 10-min incubations with TrypLE/Opti-MEM supplemented with 1 mg/ml DNase I (Sigma). The second and third extractions were combined with Dulbecco's minimal essential medium (Invitrogen) containing 10% heat inactivated horse serum (Invitrogen) and 50 units/ml penicillin plus 50 μg/ml streptomycin (Invitrogen). Cells were pelleted using centrifugation (0.5 relative centrifugal force for 5 min), resuspended in media, and plated on poly-D-lysine-coated T75 culture flasks at a density of 200,000 cells/flask. The astrocytes were cultured until reaching confluency and used for subsequent procedures as described below. Purity of astrocyte cultures (>95% pure) was periodically verified using immunocytochemistry staining protocols with an antibody against astrocytic marker glial fibrillary acidic protein (Dako, Glostrup, Denmark). The density of confluent astrocytes was ~$1 \times 10^5$ cells/cm$^2$, which were subsequently used for Western blot analysis.

*$H_2O_2$ and Zinc Treatment in Astrocytes*—Astrocytes were incubated in a serum-free medium for 3 h before exposure to $H_2O_2$. $H_2O_2$ (100 μM) (Sigma) was used to induce oxidative stress and hence enhance the Hh signaling pathway. Astrocytes then were treated by 0, 50, 100, and 150 μM $ZnCl_2$ for 40 h, where minimal zinc toxicity was observed in Live/Dead assay (Fig. 2, *C* and *D*).

*Immunoblotting*—Astrocytes were lysed on ice for 40 min in lysis buffer radioimmune precipitation assay buffer supplemented with PMSF and protease inhibitors (Cell Signaling). The lysate was centrifuged for 10 min at 4 °C and 10,000 × *g*, and then the supernatant was collected. For the culture medium, the cellular debris was separated by centrifuge at 8000 × *g* for 5 min, and then the proteins were concentrated by Centricon centrifugal concentrators (10-kDa cutoff, Amicon). The samples were mixed with SDS-PAGE sample buffer and separated by SDS-PAGE followed by immunoblotting on PVDF membrane. The membranes were blocked and incubated with a 1:100 dilution of HhN antibody (N-19, Santa Cruz Biotechnology). GADPH was used as a loading control by probing the GADPH portion of the blot in parallel with the portion containing Hh.

The autoprocessing efficiency was calculated by the following equation.

$$\text{Autoprocessing efficiency} = (I_{HhN}/M_{r\,HhN})/(I_{HhN}/M_{r\,HhN} + I_{precursor}/M_{r\,precursor}) \quad \text{(Eq. 2)}$$

where $I$ represents the gel band intensity quantified by ImageJ, and $M_r$ is molecular weight.

*Cell Viability*—Live/Dead assays were done in primary astrocyte cell culture to examine the toxicity of zinc to astrocyte cultures. Cells were incubated with 0–600 $\mu$M $ZnCl_2$ for 40 h together with 100 $\mu$M $H_2O_2$. Then cell viability was assessed using the Live/Dead cell imaging kit (Invitrogen #R37601) according to the manufacturer's directions. Stained cells were imaged using the Thermo Scientific ArrayScan XTI HCA infinity and analyzed by the Spot Detector BioApplication.

## RESULTS

*Zinc Inhibits Hh Autoprocessing In Vitro*—Hh autoprocessing consists of two steps (Fig. 1*A*). The first step is an N-S acyl shift, where Cys-1 of HhC carries out a nucleophilic attack at the carbonyl of the last residue of HhN, resulting in a thioester intermediate. Step two is cholesteroylation, where a cholesterol molecule bound to the sterol recognition region of HhC acts as a nucleophile and attacks the thioester, cleaving HhN and forming a covalent bond between the cholesterol and the C terminus of HhN. The cholesterol modification of HhN together with N-terminal palmitoylation is required for the proper secretion, transportation, and signaling of Hh ligand (26). The double-lipidated HhN binds to the membrane receptor Patched (PTCH) and activates the Hh signaling pathway (1, 27). We used a construct composed of human HhN and *Drosophila* HhC as the precursor (SHhN-DHhC) (Fig. 1*B*), which has been previously used to characterize inhibitors of Hh autoprocessing (28). The autoprocessing reaction was carried out at pH 7.1, the physiologic pH in endoplasmic reticulum where Hh autoprocessing occurs (29). In the absence of cholesterol, most precursors (HhN-HhC) remain stable, with minimal nonspecific autoprocessing (Fig. 1*C*). In the presence of cholesterol, significant amounts of separate HhN and HhC bands are observed, indicating precursor autoprocessing. The covalent attachment of cholesterol to HhN has been confirmed by LC/electrospray ionization-MS (Fig. 1*F*). With increasing concentration of zinc, more and more HhN-HhC precursor remains unprocessed, whereas less and less HhC and HhN-cholesterol is generated, demonstrating the inhibitory effect of zinc on Hh autoprocessing. Quantitation of the gel bands by ImageJ (30) and curve-fitting yields a $K_i$ of 2.3 ± 0.2 $\mu$M (Fig. 1*D*). As expected, this inhibitory effect by zinc is reversed by EDTA, a chelating agent for divalent metal (Fig. 1*E*). We also observed that zinc can inhibit Hint mediated N-S acyl shift with about $K_i$ of 14 $\mu$M (Fig. 1, *G*, *H*, and *I*), indicating zinc binding to Hint plays a major role in inhibiting cholesteroylation of the full precursor.

*Zinc Inhibits Hh Autoprocessing in Cell Culture*—To test if zinc can inhibit Hh autoprocessing in cellular environment, we used rat primary astrocytes. Astrocytes are the most abundant glial cells in the brain (31), producing Hh ligands crucial for brain development and adult neurogenesis (31–33), whereas zinc is an important signaling molecule in the nervous system (34). The Hh precursor and HhN were detected in cell lysate and in the culture medium by Western blot, respectively. Immunoblotting for GAPDH was used as a control. We found that the Hh precursors are stably expressed, but there is no observable autoprocessing (Fig. 2A) in primary astrocyte culture. In agreement with Xia *et al.* (31), incubation with 100 $\mu$M $H_2O_2$ results in the secretion of HhN into the medium, whereas Hh precursor is much weaker in cell lysate (Fig. 2*A*), indicating the autoprocessing of Hh precursor under oxidative stress. In the presence of $H_2O_2$, with increasing concentrations of zinc up to 150 $\mu$M, increasing amounts of precursor remained unprocessed, whereas decreasing the amount of HhN was released into cell culture medium (Fig. 2*A*), demonstrating the concentration-dependent inhibitory effect of zinc on Hh autoprocessing in astrocytes (Fig. 2*B*). Therefore, an increase in environmental concentration of zinc can inhibit Hh autoprocessing in cells.

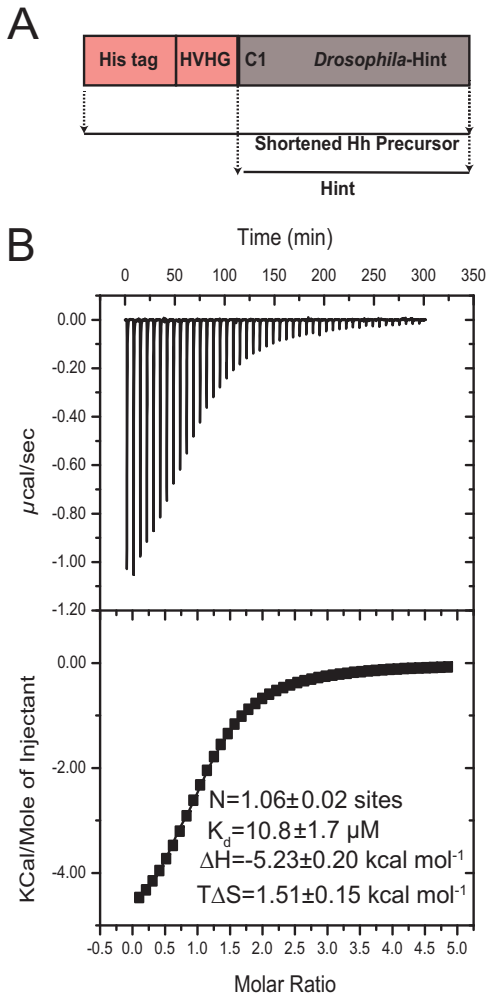


FIGURE 3. **Thermodynamics of zinc-Hint binding.** *A*, schematic diagram of the shortened precursor construct used for producing Hint sample in ITC and NMR studies. It contains a His tag and four native residues (HVHG) from HhN C terminus followed by *Drosophila melanogaster* Hint domain. The Hint domain is obtained after DTT induced cleavage from the precursor. *B*, ITC data for the titration of $Zn^{2+}$ into Hint at 25 °C. The *upper portion* contains the baseline-corrected raw data, and the *lower portion* indicates the concentration normalized heat from titration at the molar ratio of Hint.

To examine the zinc toxicity, we carried out Live/Dead assays on astrocyte cultures under 0–600 $\mu$M $ZnCl_2$ treatment. When zinc concentrations were 150 $\mu$M or smaller, cell viabilities were largely unchanged. Zinc concentrations of 200 $\mu$M and above caused substantial cell death, which is consistent with previous reports (Fig. 2, *C* and *D*) (35, 36).

*Thermodynamics of Zinc-Hint Binding*—This has been determined with ITC (Fig. 3*B*). Because zinc most likely binds

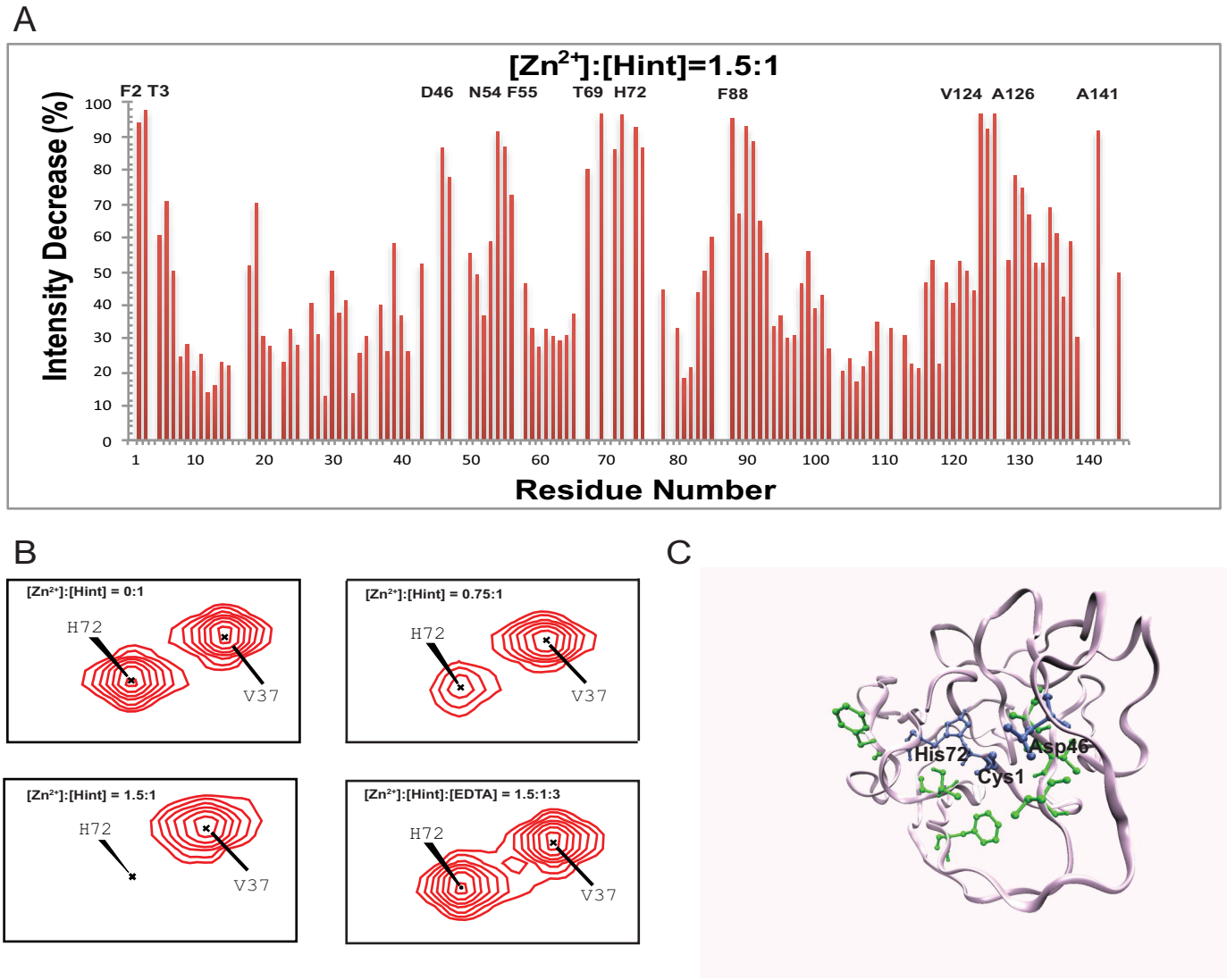


FIGURE 4. **Structural basis of zinc-Hint binding.** *A*, $^{1}H,^{15}N$-HSQC signal intensity changes of $Zn^{2+}$ binding to Hint at 25 °C. The residues with the biggest changes are labeled. *B*, chemical shift perturbation analysis for His-72 backbone in $^{15}N$-labeled Hint upon zinc binding. With increasing amount of zinc, the amide peak intensities of His-72 decreased during the titration. Adding 2 mol eq of EDTA resulted in the complete reappearance of the missing signals. *C*, structural model of Hint binding site of $Zn^{2+}$ mapped onto the x-ray structure (PDB ID 1AT0) based on the NMR signal intensity change. *Blue residues* are the direct coordination sites, which have the biggest signal decrease, whereas *green residues*, with less signal reduction, likely play a secondary role in zinc binding.

to the Hint domain of Hh, the ITC is carried out with the *Drosophila* Hint domain at pH 7.1 at 298 K. Fitting of the isotherm in Fig. 3*B* resulted in the binding stoichiometry ($n$) of 1.06 ± 0.02 and $K_d$ of 11 ± 2 μM from three repeated measurements. The values of the $\Delta H$ (−5.2 ± 0.2 kcal mol$^{-1}$) and T$\Delta$S (1.5 ± 0.2 kcal mol$^{-1}$) indicate zinc binding to Hint is both enthalpically and entropically favorable, with $\Delta H$ being the main driving factor.

*Zinc Binds to Active Site Residues in Hint*—We mapped the zinc binding sites in Hint domain with $^{1}H,^{15}N$-HSQC spectra of Hint (Fig. 4, *A* and *B*), as Hint contains the key catalytic residues for Hh autoprocessing (13). The complete backbone and aliphatic side chain assignment of Hint has been published (22). The NMR signals of many amides decreased with the zinc titration (Fig. 4, *A* and *B*), such as Phe-2, Thr-3, Asp-46, Asn-54, Phe-55, Thr-69, His-72, Phe-88, Val-124, Ala-126, and Ala-141, due to chemical exchange broadening. The peaks with strongest reduction in peak intensity are likely at or close to the zinc coordination sites. When mapped onto the three-dimensional structure of Hint (13), all the residues with the largest signal reductions were close to three conserved catalytic residues Cys-1, Asp-46, and His-72 (Fig. 4*C*). Cysteine, aspartate, and histidine residues are the most common sites for zinc coordination in proteins (37). To further confirm the coordination role of these three residues, we also conducted zinc titration with $^{13}C,^{1}H$-HSQC. Because Cys-1 is the first residue at the N terminus of Hint and has a very fast exchange rate with the solvent, the Cys-1 amide is not detectable with $^{1}H,^{15}N$-HSQC. In $^{13}C,^{1}H$-HSQC, we observed strong NMR signals for Cys-1 side chain (Fig. 5*A*), which disappeared upon zinc binding (Fig. 5*A*). Similar signal reductions upon zinc binding were also observed for Asp-46 and His-72 side chains (Fig. 5, *B* and *C*). In all experiments, the NMR signals affected by zinc reappeared upon the addition of EDTA (Fig. 5). These results establish that the Cys-1, Asp-46, and His-72 are likely zinc coordination sites in Hint. Because these three residues play a key role in Hh auto-

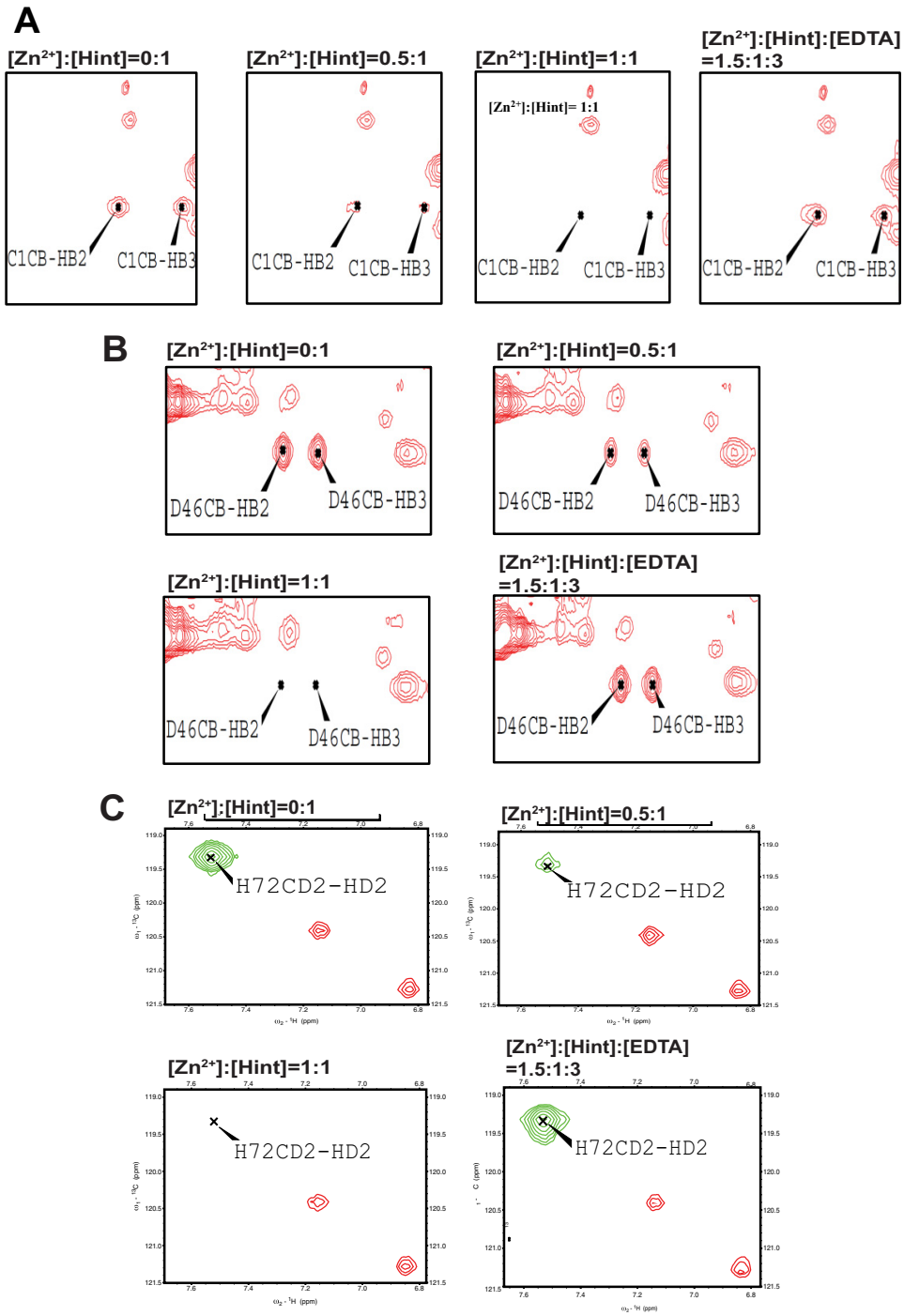


FIGURE 5. **NMR studies of side-chain binding to zinc using $^{13}C$ NMR experiments.** *A*, the effect of $Zn^{2+}$ titration on the Cys-1 side chain monitored by $^{13}C$-aliphatic HSQC, which can be reversed by adding EDTA. *B*, the effect of $Zn^{2+}$ titration on the Asp-46 side chain by $^{13}C$-aliphatic HSQC, which can be reversed by adding EDTA. *C*, the effect of $Zn^{2+}$ titration on the His-72 side chain by $^{13}C$-aromatic HSQC, which also can be reversed by adding EDTA.

processing (13), when zinc binds to these three residues, the active site geometry and mobility will be perturbed, compromising their catalytic efficiency.

## DISCUSSION

Zinc is an essential trace element, acting as a co-factor for >300 enzymes that regulate a variety of cellular processes and signaling pathways (38). Zinc is also a signaling molecule and can modulate synaptic activity (39). The imbalance of zinc homeostasis has been established in many pathological conditions (14–21), including many types of cancer and autism. However, the mechanistic role of zinc deficiency in these diseases remains poorly understood.

Based on our data, we propose that there is a mechanistic link between zinc deficiency and Hh-ligand-dependent activation of the Hh signaling pathway in three types of cancers, prostate cancer, lung cancer, and ovarian cancer. Lung cancer is the leading cause of death. Prostate cancer is the second most com-

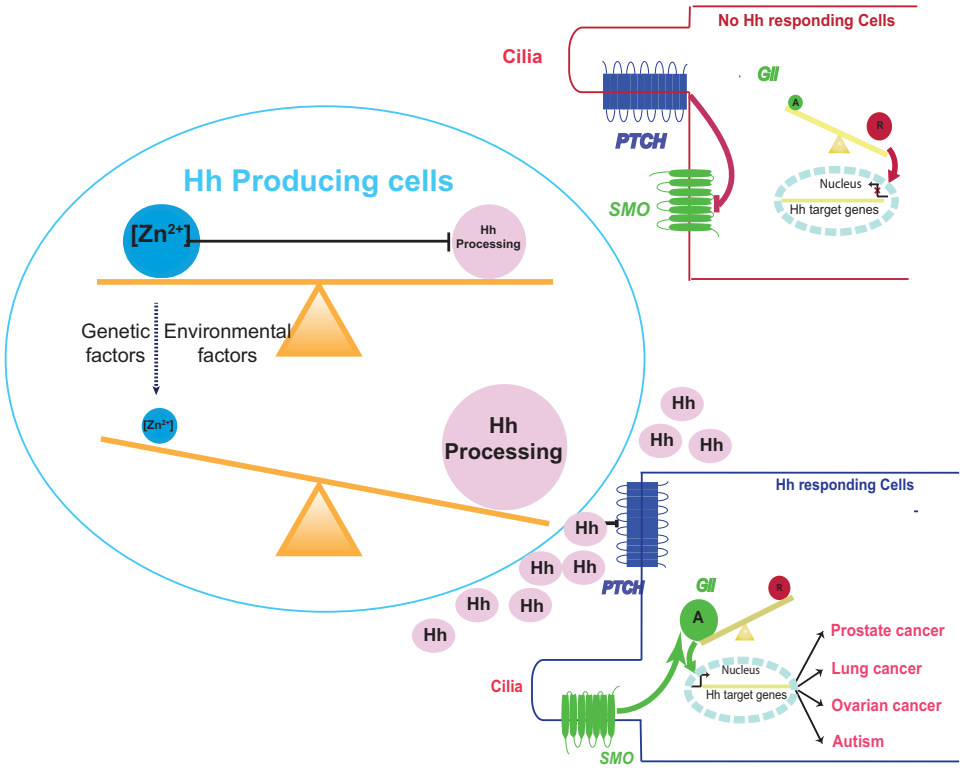


FIGURE 6. **A new pathway in diseases; zinc deficiency leads to overproduction of Hh ligand and the activation of Hh signaling pathway.** Under normal physiological conditions, zinc binds to Hint domain on Hh precursor and inhibits Hh autoprocessing and Hh signaling pathway. When the zinc level is low, Hh autoprocessing will be enhanced, leading to overproduction of Hh ligand. Hh ligand binds to Patched (*PTCH*), relieving its inhibition of Smoothened (*SMO*). Smoothened in turn activates Gli transcription factors, turning on the transcriptions of Hh target genes. The low zinc-high Hh axis may contribute to the pathogenic mechanisms of many types of cancer and ASD.

mon cancer in man, whereas ovarian cancer is the leading cause of death from gynecologic malignancy. In these three cancers Hh ligand is overproduced resulting in abnormal activation of Hh signaling pathway (2–8), whereas zinc deficiency has also been clearly established (14–21). The zinc level in the human prostate is the highest among any soft tissue in the healthy body. Decrease in zinc is observed early in the course of prostate cancer development, and the trend continues toward castration-resistant disease (40). Several studies showed the depression of zinc concentration in the cancerous human lung tissues, especially in the small cell lung cancer, the most malignant form in lung cancer (17, 19, 41). For ovarian cancer, serum zinc decreased in patients subsequently diagnosed with ovarian cancer, whereas in tumor tissue, the concentration of zinc also decreased (20, 21). However, the precise pathogenic role of zinc deficiency is not known in these cancers. Our *in vitro* and cell culture experiments (Figs. 1 and 2) demonstrated that zinc inhibits Hh autoprocessing. These data suggest that low zinc in tissues can enhance Hh autoprocessing and generate more Hh ligand; thus, zinc deficiency can be a novel mechanism of Hh ligand overproduction in these cancers. Hh pathway inhibitors targeting the downstream receptor Smoothened (SMO) have recently generated much excitement as a novel type of therapy for cancer (11). However, drug resistance to SMO inhibitors is already emerging (42), and SMO inhibitors are not effective against tumors driven by overproduction of Hh ligand (11). Our data suggest targeting the upstream autoprocessing of Hh may be an important alternative for inhibiting Hh pathway in diseases, particularly those driven by high levels of Hh ligand. Our biophysical studies of zinc-Hh interaction will contribute to rational design of inhibitors of Hh autoprocessing.

ASD, with an astounding prevalence of ~2% (43), is characterized by abnormal social interaction, communication, and stereotyped behaviors in affected children. The etiology of ASD is poorly understood, but both oxidative stress (44) and low zinc status have been reproducibly associated with ASD (16, 45). In astrocyte culture, Hh autoprocessing is promoted by $H_2O_2$ and low zinc level (Fig. 2*A*), offering a plausible mechanistic explanation for the recent observation of increased serum level of sonic Hh ligand in ASD (9). The resulting higher level of secreted Hh ligand may lead to the abnormal activation of Hh signaling pathway in both neurons and glial cells in the developing brain. A clinical feature of ASD, macrocephaly, also implicates Hh activation (46–48). Hh plays an important role in the early expansion of the developing brain and in regulating the cerebral cortical size (49, 50). In contrast, the opposite clinical feature, microcephaly, is observed in holoprosencephaly (51), which can be caused by mutations in the Hh autoprocessing domain (HhC) that reduce Hh ligand production (51–54). The abnormal activation of Hh pathway, even transiently by fluctuations in zinc level, may cause brain overgrowth, disrupting the proper development of neuronal network for language and social interactions. We, therefore, hypothesize that in ASD low zinc status promotes Hh autoprocessing and the generation of higher level of Hh ligand. Coupled with oxidative and/or genetic defects in other Hh signaling components, low zinc sta-

tus may lead to abnormal activation of Hh signaling pathway during brain development, contributing to the complex etiology of ASD.

There is an apparent discrepancy between nanomolar levels of concentration of free zinc in cytosol and endoplasmic reticulum (55–58) where Hh autoprocessing occurs, and the $\mu$M $K_i$ of zinc inhibition of Hh autoprocessing measured *in vitro*. A similar unresolved conundrum exists in many zinc transporters whose measured $K_m$ values are in the $\mu$M range (59–63). Yet they have to transport zinc in an environment with ~nM free zinc concentration. For Hh autoprocessing, one possibility is that the local concentration of zinc near plasma membrane is much higher than the measured values. The spatial and temporal distribution of zinc within endoplasmic reticulum is likely to be uneven and dynamic. Hh precursor, bound to the hydrophobic cholesterol is likely to be close to or associated with organelle membrane, where active zinc transport occurs and available zinc is enriched. In addition, HhN also binds zinc (64), further increasing the effective concentration of Zn for the inhibition of Hh autoprocessing. Alternatively, the endoplasmic reticulum environment may decrease $K_i$ dramatically through an unknown mechanism. Lastly, we cannot completely rule out the possibility that zinc inhibits Hh autoprocessing through an indirect signaling effect because of the ubiquitous presence of zinc in many proteins and its signaling roles.

In summary, we have linked Hh signal transduction pathways, important in both development and diseases, with a ubiquitous trace element zinc through the novel discovery that zinc binds directly to the Hint domain and inhibits Hh autoprocessing, as shown both *in vitro* and in cell culture. Because both zinc and Hh play crucial roles in many aspects of human physiology and diseases, the implication of our finding is profound. When zinc levels are low, Hh autoprocessing may be enhanced, leading to overproduction of Hh ligand and potentially abnormal activation of Hh signaling pathway. This low zinc-high Hh axis may contribute to the pathogenic mechanisms of many types of cancer and ASD (Fig. 6). Our data not only provide novel etiological insights for these diseases but also point to new ways to diagnose and treat diseases by combined measurement and manipulation of zinc level and Hh autoprocessing. Future directions include in-depth investigation of the correlation between zinc level and Hh autoprocessing in selected diseases and further clarification of zinc binding and inhibition mechanism with mutagenesis and structure determination.

## REFERENCES


1. Briscoe, J., and Thérond, P. P. (2013) The mechanisms of Hedgehog signalling and its roles in development and disease. *Nat. Rev. Mol. Cell Biol.* **14,** 416–429
2. Karhadkar, S. S., Bova, G. S., Abdallah, N., Dhara, S., Gardner, D., Maitra, A., Isaacs, J. T., Berman, D. M., and Beachy, P. A. (2004) Hedgehog signalling in prostate regeneration, neoplasia, and metastasis. *Nature* **431,** 707–712
3. Sanchez, P., Hernández, A. M., Stecca, B., Kahler, A. J., DeGueme, A. M., Barrett, A., Beyna, M., Datta, M. W., Datta, S., and Ruiz i Altaba, A. (2004) Inhibition of prostate cancer proliferation by interference with Sonic Hedgehog-Gli1 signaling. *Proc. Natl. Acad. Sci. U.S.A.* **101,** 12561–12566
4. Sheng, T., Li, C., Zhang, X., Chi, S., He, N., Chen, K., McCormick, F., Gatalica, Z., and Xie, J. (2004) Activation of the hedgehog pathway in advanced prostate cancer. *Mol. Cancer* **3,** 29
5. Watkins, D. N., Berman, D. M., Burkholder, S. G., Wang, B., Beachy, P. A., and Baylin, S. B. (2003) Hedgehog signalling within airway epithelial progenitors and in small-cell lung cancer. *Nature* **422,** 313–317
6. Velcheti, V., and Govindan, R. (2007) Hedgehog signaling pathway and lung cancer. *J. Thorac. Oncol.* **2,** 7–10
7. Chen, X., Horiuchi, A., Kikuchi, N., Osada, R., Yoshida, J., Shiozawa, T., and Konishi, I. (2007) Hedgehog signal pathway is activated in ovarian carcinomas, correlating with cell proliferation: its inhibition leads to growth suppression and apoptosis. *Cancer Sci.* **98,** 68–76
8. Liao, X., Siu, M. K., Au, C. W., Wong, E. S., Chan, H. Y., Ip, P. P., Ngan, H. Y., and Cheung, A. N. (2009) Aberrant activation of hedgehog signaling pathway in ovarian cancers: effect on prognosis, cell invasion, and differentiation. *Carcinogenesis* **30,** 131–140
9. Al-Ayadhi, L. Y. (2012) Relationship between Sonic hedgehog protein, brain-derived neurotrophic factor, and oxidative stress in autism spectrum disorders. *Neurochem. Res.* **37,** 394–400
10. Pepinsky, R. B., Zeng, C., Wen, D., Rayhorn, P., Baker, D. P., Williams, K. P., Bixler, S. A., Ambrose, C. M., Garber, E. A., Miatkowski, K., Taylor, F. R., Wang, E. A., and Galdes, A. (1998) Identification of a palmitic acid-modified form of human sonic hedgehog. *J. Biol. Chem.* **273,** 14037–14045
11. Atwood, S. X., and Oro, A. E. (2014) "Atypical" regulation of hedgehog-dependent cancers. *Cancer Cell* **25,** 133–134
12. Zhang, L., Zheng, Y., Xi, Z., Luo, Z., Xu, X., Wang, C., and Liu, Y. (2009) Metal ions binding to recA inteins from *Mycobacterium tuberculosis*. *Mol. Biosyst.* **5,** 644–650
13. Hall, T. M., Porter, J. A., Young, K. E., Koonin, E. V., Beachy, P. A., and Leahy, D. J. (1997) Crystal structure of a Hedgehog autoprocessing domain: homology between Hedgehog and self-splicing proteins. *Cell* **91,** 85–97
14. Costello, L. C., and Franklin, R. B. (2011) Zinc is decreased in prostate cancer: an established relationship of prostate cancer! *J. Biol. Inorg. Chem.* **16,** 3–8
15. Lakshmi Priya, M. D., and Geetha, A. (2011) Level of trace elements (copper, zinc, magnesium and selenium) and toxic elements (lead and mercury) in the hair and nail of children with autism. *Biol. Trace Elem. Res.* **142,** 148–158
16. Bjorklund, G. (2013) The role of zinc and copper in autism spectrum disorders. *Acta Neurobiol. Exp. (Wars)* **73,** 225–236
17. Braziewicz, J., Bana, D., Majewska, U., and Urbaniak, A. (1999) Trace element load in cancer and normal lung tissue. *Nucl. Instrum. Methods Phys. Res. B* **150,** 193–199
18. Zhang, L., Lv, J., and Sun, S. (2012) Elements in lung tissues of patients from a high lung cancer incidence area of China. *Biol. Trace Elem. Res.* **148,** 7–10
19. Gumulec, J., Masarik, M., Adam, V., Eckschlager, T., Provaznik, I., and Kizek, R. (2014) Serum and tissue zinc in epithelial malignancies: a meta-analysis. *PLoS ONE* **9,** e99790
20. Blnur, N., Drugan, A., and Brandes, M. (1986) Use of the serum copper/zinc malignancy. *Clin. Chem.* **32,** 101–103
21. Memon, A.-R., Kazi, T. G., Afridi, H. I., Jamali, M. K., Arain, M. B., Jalbani, N., and Syed, N. (2007) Evaluation of zinc status in whole blood and scalp hair of female cancer patients. *Clin. Chim. Acta* **379,** 66–70
22. Xie, J., Du, Z., Callahan, B., Belfort, M., and Wang, C. (2014) $^{1}$H, $^{13}$C, and $^{15}$N NMR assignments of a *Drosophila* Hedgehog autoprocessing domain. *Biomol. NMR Assign.* **8,** 279–281
23. Delaglio, F., Grzesiek, S., Vuister, G. W., Zhu, G., Pfeifer, J., and Bax, A. (1995) NMRPipe: A multidimensional spectral processing system based on UNIX pipes. *J. Biomol. NMR* **6,** 277–293
24. Zuidema, J. M., Hyzinski-García, M. C., Van Vlasselaer, K., Zaccor, N. W., Plopper, G. E., Mongin, A. A., and Gilbert, R. J. (2014) Enhanced GLT-1 mediated glutamate uptake and migration of primary astrocytes directed by fibronectin-coated electrospun poly-L-lactic acid fibers. *Biomaterials* **35,** 1439–1449
25. Mongin, A. A., Hyzinski-García, M. C., Vincent, M. Y., and Keller, R. W., Jr. (2011) A simple method for measuring intracellular activities of glutamine synthetase and glutaminase in glial cells. *Am. J. Physiol. Cell Physiol.* **301,** C814–C822
26. Chamoun, Z., Mann, R. K., Nellen, D., von Kessler, D. P., Bellotto, M.,

Beachy, P. A, and Basler, K. (2001) Skinny hedgehog, an acyltransferase required for palmitoylation and activity of the hedgehog signal. *Science* **293,** 2080–2084
27. Taipale, J., Cooper, M. K., Maiti, T., and Beachy, P. A. (2002) Patched acts catalytically to suppress the activity of Smoothened. *Nature* **418,** 892–897
28. Owen, T. S., Xie, X. J., Laraway, B., Ngoje, G., Wang, C., and Callahan, B. P. (2015) Active site targeting of hedgehog precursor protein with phenylarsine oxide. *Chembiochem* **16,** 55–58
29. Chen, X., Tukachinsky, H., Huang, C.-H., Jao, C., Chu, Y.-R., Tang, H.-Y., Mueller, B., Schulman, S., Rapoport, T. A, and Salic, A. (2011) Processing and turnover of the Hedgehog protein in the endoplasmic reticulum. *J. Cell Biol.* **192,** 825–838
30. Abràmoff, M. D., Hospitals, I., Magalhães, P. J., and Abràmoff, M. (2004) Image Processing with ImageJ. *Biophotonics International* 1–7
31. Xia, Y.-P., Dai, R.-L., Li, Y.-N., Mao, L., Xue, Y.-M., He, Q.-W., Huang, M., Huang, Y., Mei, Y.-W., and Hu, B. (2012) The protective effect of sonic hedgehog is mediated by the phosphoinositide [corrected] 3-kinase/AKT/Bcl-2 pathway in cultured rat astrocytes under oxidative stress. *Neuroscience* **209,** 1–11
32. Cai, C., Thorne, J., and Grabel, L. (2008) Hedgehog serves as a mitogen and survival factor during embryonic stem cell neurogenesis. *Stem Cells* **26,** 1097–1108
33. Han, Y.-G., Spassky, N., Romaguera-Ros, M., Garcia-Verdugo, J.-M., Aguilar, A., Schneider-Maunoury, S., and Alvarez-Buylla, A. (2008) Hedgehog signaling and primary cilia are required for the formation of adult neural stem cells. *Nat. Neurosci.* **11,** 277–284
34. Segawa, S., Nishiura, T., Furuta, T., Ohsato, Y., Tani, M., Nishida, K., and Nagasawa, K. (2014) Zinc is released by cultured astrocytes as a gliotransmitter under hypoosmotic stress-loaded conditions and regulates microglial activity. *Life Sci.* **94,** 137–144
35. Bishop, G. M., Dringen, R., and Robinson, S. R. (2007) Zinc stimulates the production of toxic reactive oxygen species (ROS) and inhibits glutathione reductase in astrocytes. *Free Radic. Biol. Med.* **42,** 1222–1230
36. Nolte, C., Gore, A., Sekler, I., Kresse, W., Hershfinkel, M., Hoffmann, A., Kettenmann, H., and Moran, A. (2004) ZnT-1 expression in astroglial cells protects against zinc toxicity and slows the accumulation of intracellular zinc. *Glia* **48,** 145–155
37. Maret, W. (2012) New perspectives of zinc coordination environments in proteins. *J. Inorg. Biochem.* **111,** 110–116
38. Szewczyk, B. (2013) Zinc homeostasis and neurodegenerative disorders. *Front. Aging Neurosci.* **5,** 33
39. Yamasaki, S., Sakata-Sogawa, K., Hasegawa, A., Suzuki, T., Kabu, K., Sato, E., Kurosaki, T., Yamashita, S., Tokunaga, M., Nishida, K., and Hirano, T. (2007) Zinc is a novel intracellular second messenger. *J. Cell Biol.* **177,** 637–645
40. Kolenko, V., Teper, E., Kutikov, A., and Uzzo, R. (2013) Zinc and zinc transporters in prostate carcinogenesis. *Nat. Rev. Urol.* **10,** 219–226
41. Carvalho, M. L., Magalhães, T., Becker, M., and von Bohlen, A. (2007) Trace elements in human cancerous and healthy tissues: a comparative study by EDXRF, TXRF, synchrotron radiation, and PIXE. *Spectrochim. Acta Part B. At. Spectrosc.* **62,** 1004–1011
42. Yauch, R. L., Dijkgraaf, G. J., Alicke, B., Januario, T., Ahn, C. P., Holcomb, T., Pujara, K., Stinson, J., Callahan, C. A., Tang, T., Bazan, J. F., Kan, Z., Seshagiri, S., Hann, C. L., Gould, S. E., Low, J. A., Rudin, C. M., and de Sauvage, F. J. (2009) Smoothened mutation confers resistance to a Hedgehog pathway inhibitor in medulloblastoma. *Science* **326,** 572–574
43. Blumberg, S. J., and Bramlett, M. D. (2013) *Changes in Prevalence of Parent-reported Autism Spectrum Disorder in School-aged U. S. Children: 2007 to 2011–2012. National Health Statistics Reports* **65,** 1–12
44. McGinnis, W. R. (2005) Oxidative stress in autism. *Altern. Ther. Health Med.* **11,** 19
45. Grabrucker, A. M. (2012) Environmental factors in autism. *Front. Psychiatry* **3,** 118
46. Redcay, E., and Courchesne, E. (2005) When is the brain enlarged in autism? A meta-analysis of all brain size reports. *Biol. Psychiatry* **58,** 1–9
47. Elder, L. M., Dawson, G., Toth, K., Fein, D., and Munson, J. (2008) Head circumference as an early predictor of autism symptoms in younger siblings of children with autism spectrum disorder. *J. Autism Dev. Disord.* **38,** 1104–1111
48. White, S., O'Reilly, H., and Frith, U. (2009) Big heads, small details, and autism. *Neuropsychologia* **47,** 1274–1281
49. Lien, W.-H., Klezovitch, O., Fernandez, T. E., Delrow, J., and Vasioukhin, V. (2006) alphaE-catenin controls cerebral cortical size by regulating the hedgehog signaling pathway. *Science* **311,** 1609–1612
50. Britto, J., Tannahill, D., and Keynes, R. (2002) A critical role for sonic hedgehog signaling in the early expansion of the developing brain. *Nat. Neurosci.* **5,** 103–110
51. Nanni, L., Ming, J. E., Bocian, M., Steinhaus, K., Bianchi, D. W., Die-Smulders, C., Giannotti, A., Imaizumi, K., Jones, K. L., Campo, M. D., Martin, R. A., Meinecke, P., Pierpont, M. E., Robin, N. H., Young, I. D., Roessler, E., and Muenke, M. (1999) The mutational spectrum of the sonic hedgehog gene in holoprosencephaly: SHH mutations cause a significant proportion of autosomal dominant holoprosencephaly. *Hum. Mol. Genet.* **8,** 2479–2488
52. Belloni, E., Muenke, M., Roessler, E., Traverso, G., Siegel-Bartelt, J., Frumkin, A., Mitchell, H. F., Donis-Keller, H., Helms, C., Hing, A. V., Heng, H. H., Koop, B., Martindale, D., Rommens, J. M., Tsui, L. C., and Scherer, S. W. (1996) Identification of Sonic hedgehog as a candidate gene responsible for holoprosencephaly. *Nat. Genet.* **14,** 353–356
53. Roessler, E., Belloni, E., Gaudenz, K., Vargas, F., Scherer, S. W., Tsui, L. C., and Muenke, M. (1997) Mutations in the C-terminal domain of Sonic Hedgehog cause holoprosencephaly. *Hum. Mol. Genet.* **6,** 1847–1853
54. Maity, T., Fuse, N., and Beachy, P. A (2005) Molecular mechanisms of Sonic hedgehog mutant effects in holoprosencephaly. *Proc. Natl. Acad. Sci. U.S.A.* **102,** 17026–17031
55. Vinkenborg, J. L., Nicolson, T. J., Bellomo, E. A., Koay, M. S., Rutter, G. A., and Merkx, M. (2009) Genetically encoded FRET sensors to monitor intracellular $Zn^{2+}$ homeostasis. *Nat. Methods* **6,** 737–740
56. Chabosseau, P., Tuncay, E., Meur, G., Bellomo, E. A., Hessels, A., Hughes, S., Johnson, P. R., Bugliani, M., Marchetti, P., Turan, B., Lyon, A. R., Merkx, M., and Rutter, G. A. (2014) Mitochondrial and ER-Targeted eCALWY Probes Reveal High Levels of Free $Zn^{2+}$. *ACS Chem. Biol.* **9,** 2111–2120
57. Hessels, A. M., and Merkx, M. (2015) Genetically-encoded FRET-based sensors for monitoring $Zn^{2+}$ in living cells. *Metallomics* **7,** 258–266
58. Bellomo, E. A., Meur, G., and Rutter, G. A (2011) Glucose regulates free cytosolic $Zn^{2+}$ concentration, Slc39 (ZiP), and metallothionein gene expression in primary pancreatic islet $\beta$-cells. *J. Biol. Chem.* **286,** 25778–25789
59. Gaither, L. A., and Eide, D. J. (2001) The human ZIP1 transporter mediates zinc uptake in human K562 erythroleukemia cells. *J. Biol. Chem.* **276,** 22258–22264
60. Dufner-Beattie, J., Wang, F., Kuo, Y.-M., Gitschier, J., Eide, D., and Andrews, G. K. (2003) The acrodermatitis enteropathica gene ZIP4 encodes a tissue-specific, zinc-regulated zinc transporter in mice. *J. Biol. Chem.* **278,** 33474–33481
61. Gaither, L. A. (2000) Functional expression of the human hZIP2 zinc transporter. *J. Biol. Chem.* **275,** 5560–5564
62. Eide, D. J. (2006) Zinc transporters and the cellular trafficking of zinc. *Biochim. Biophys. Acta* **1763,** 711–722
63. Dufner-Beattie, J., Langmade, S. J., Wang, F., Eide, D., and Andrews, G. K. (2003) Structure, function, and regulation of a subfamily of mouse zinc transporter genes. *J. Biol. Chem.* **278,** 50142–50150
64. Hall, T. M., Porter, J. A., Beachy, P. A., and Leahy D. J. (1995) A potential catalytic site revealed by the 1.7-Å crystal structure of the amino-terminal signalling domain of sonic hedgehog. *Nature* **378,** 212–216